第 33 卷第 10 期　　焊　接　学　报　　Vol. 33　No. 10
2012 年 10 月　　TRANSACTIONS OF THE CHINA WELDING INSTITUTION　　October　2012

考虑热损失的热丝 TIG 焊热丝温度分布解析模型

赵福海[1,2]，　华学明[1,2]，　叶　欣[1,2]，　吴毅雄[1,2,3]

(1. 上海交通大学 材料科学与工程学院，200240；2. 上海交通大学 上海市激光制造与材料改性重点实验室，200240；
3. 上海交通大学 金属基复合材料国家重点实验室，上海　200240)

赵福海

摘　要：基于能量守恒定律建立了考虑热损失的电阻加热热丝温度分布的数学解析模型，验证了此解析模型的计算结果与文献中的实测数据的基本吻合性，并讨论了焊丝直径、热丝电流、送丝速度以及焊丝伸出长度等因素对热丝温度分布的影响规律. 结果表明，此数学解析模型具有很高的准确性，可以用来进行热丝加热过程的分析以及焊接质量的控制；焊丝直径越小、热丝电流越大、送丝速度越小，焊丝伸出部分上距给电点相同距离的温度越高；焊丝伸出长度越大，焊丝伸出部分距焊丝送入位置相同距离的温度越高.

关键词：热丝钨极氩弧焊；　热损失；　热丝温度；　解析模型

中图分类号：TG444　　**文献标识码**：A　　**文章编号**：0253－360X(2012)10－0097－04

0　序　　言

热丝 TIG 焊是在传统 TIG 焊基础上发展起来的一种优质、高效、节能的焊接工艺，其基本原理是在焊丝送进熔池之前对其进行加热，使其达到一定的预热温度，最后在熔池传热的作用下使其熔化，作为填充金属进入熔池. 这种焊接方法扩大了传统 TIG 焊工艺方法的适应性与应用范围，具有较高的经济价值. 日本广岛大学的 Shinozaki1，Yamamoto 等人[1－3]的研究表明，热丝 TIG 焊焊丝温度分布对焊缝成形与焊接质量的影响非常大. 而精确控制焊丝温度分布是保证热丝 TIG 焊质量的关键，从而对焊丝温度分布进行数学建模. Shinozaki，Yamamoto 等人[4,5]利用辐射温度计对焊丝温度分布进行了测量，并对焊丝温度分布进行了估算. TIG 焊焊丝温度分布影响因素众多，加大了对热丝 TIG 焊焊丝温度分布研究的困难，目前在此方面的研究甚少. 文中以 SUS3－系列奥氏体不锈钢焊丝为例，拟建立热丝温度分布数学解析模型，并验证其准确性，对焊丝温度分布影响因素进行分析讨论.

1　热丝 TIG 焊热丝温度分布解析模型

为了简化温度场解析模型，事先做出如下假设：(1) 由于焊丝较细，忽略其径向方向上的温度差异，只考虑其在焊丝伸出长度方向上一维的温度分布；(2) 在整个焊丝加热过程中，焊丝的物性参数不随温度变化；(3) 焊丝的初始温度分布是均匀的，并且不考虑相变和结晶潜热.

热丝 TIG 焊焊丝伸出长度部分的加热简图如图 1 所示. 设焊丝伸出长度为 L，送丝速度为 v，焊丝的初始温度分布为 T_0，则焊丝从给电点 O 运动到焊丝熔化点 A 处所用时间为 L/v，焊丝被逐渐加热.

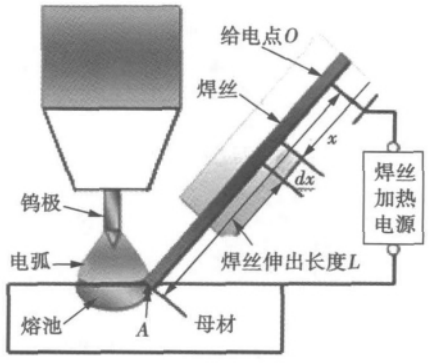

图 1　热丝 TIG 焊焊丝伸出部分加热示意图

Fig. 1　Schematic diagram of wire-heated by resistance heat during hot-wire TIG welding process

热丝 TIG 焊热丝温度分布满足如下的控制方程和边界条件

$$\frac{\lambda}{c\rho}\frac{\partial^2 T}{\partial x^2}+v\frac{\partial T}{\partial x}+\frac{j^2\sigma}{c\rho}-\frac{2\beta}{c\rho r}(T-T_f)=0 \qquad (1)$$

边界条件：$T(0)=T_m$

收稿日期：2011－08－28

$$T(L) = T_0$$

式中: c 为比热容 J/(kg·K); ρ 为密度, kg/m^3; v 为送丝速度, m/s; r 为焊丝半径 m; T_f 为环境温度, K; λ 为热导率, W/(m·K); j 为电流密度, A/m^2; σ 为焊丝的电阻率 Ω·m; h 为焊丝的对流散热系数, W/(m^2·K); δ 为 Stefan-Boltzman 常数, W/(m^2·K^4); ε 为表面辐射系数; T_0 为焊丝的初始温度, K; T_m 为焊丝的熔点, K; L 为焊丝伸出长度, m.

式(1)中的第一项为热传导项; 第二项由于焊丝被送入熔池而导致的对流项; 第三项是将焦耳热作为内热源; 第四项为由于焊丝与周围空气的热对流而散失的热量; 第五项为由于热辐射而散失的热量.

式(1)与文献[7,8]中对 GMAW 焊丝加热过程分析讨论时所用的控制方程类似, 但是文献[7,8]均未考虑焊丝与周围环境因热对流和热辐射而损失的热量, 即不含有式(1)中的第四项和第五项.

为了求出式(1)定解问题的解析解, 将式(1)中的第四项和第五项用一个式子来表示, 即

$$\frac{2}{r}h(T-T_f) - \frac{2}{r}\delta\varepsilon(T^4 - T_f^4) = \frac{2}{r}\alpha(T-T_f) \quad (2)$$

式中: α 为表面散热系数 W/(m^2·K).

式(1)则化为如下形式, 即

$$\lambda\frac{\partial^2 T}{\partial x^2} + c\rho v\frac{\partial T}{\partial x} + j^2\sigma - \frac{2}{r}\alpha(T-T_f) = 0 \quad (3)$$

边界条件: $T(0) = T_m$

$$T(L) = T_0$$

利用变量代换的方法对式(3)进行变换, 即令

$$\theta = T - T_f$$

则有

$$k\frac{\partial^2\theta}{\partial x^2} + v\frac{\partial\theta}{\partial x} - \frac{2\alpha}{c\rho r}\theta + \frac{j^2\sigma}{c\rho} = 0 \quad (4)$$

边界条件: $\theta(0) = T_m - T_f$

$$\theta(L) = T_0 - T_f$$

对含边界条件的式(4)的定解问题, 可求得其解析解. 所以考虑热损失的热丝 TIG 焊热丝准稳态温度分布的解析模型为

$$T = \left[\begin{array}{l}\left(T_m - T_f - \dfrac{j^2\sigma r}{2\alpha}\right)\left(\mathrm{e}^{(\lambda_2 L + \lambda_1 x)} - \mathrm{e}^{(\lambda_1 L + \lambda_2 x)}\right) \\ -\left(T_0 - T_f - \dfrac{j^2\sigma r}{2\alpha}\right)\left(\mathrm{e}^{\lambda_1 x} - \mathrm{e}^{\lambda_2 x}\right)\end{array}\right] / \left(\mathrm{e}^{\lambda_2 L} - \mathrm{e}^{\lambda_1 L}\right) + \frac{j^2\sigma r}{2\alpha} + T_f \quad (5)$$

式中: $\lambda_1 = \dfrac{-v - \sqrt{v^2 + 8k\alpha/c\rho r}}{2k}$

$$\lambda_2 = \frac{-v + \sqrt{v^2 + 8k\alpha/c\rho r}}{2k}$$

2 解析模型的验证与讨论

2.1 热丝温度分布数学模型的验证

2.1.1 模型中材料物性参数的选取以及 α 的确定

根据文献[4], [6], 选取 SUS3 系列奥氏体不锈钢的热物理参数如表 1 所示.

表 1 SUS3 系列的热物理参数的选取值

Table 1 Values of thermo-physical properties of SUS3 stainless steel

比热容 c/(J·kg^{-1}·K)	热导率 λ/(W·m^{-1}·K)	密度 ρ/(kg·m^{-3})	熔点 T_m/K	对流换热系数 h/(W·m^{-2}·K)	Stefan-Boltzman 常数 δ/(W·m^{-2}·K^4)	表面辐射系数 ε
479	16.3	7 200	1 727	80	5.67×10^{-8}	0.4

由斯蒂芬波尔兹曼定律可得, 单位时间、单位面积因辐射传热而损失的热流密度为

$$q_{\mathrm{rad}} = \delta\varepsilon(T^4 - T_f^4)$$

利用泰勒一阶展开式来对上式进行线性化处理

$$T^4 \approx T_f^4 + 4T_f^3(T - T_f)$$

所以, $q_{\mathrm{rad}} = 4\delta\varepsilon T_f^3(T - T_f)$

$$q_{\text{heat-loss}} \approx h(T - T_f) + 4\delta\varepsilon T_f^3(T - T_f)$$

$$\alpha \approx h + 4\delta\varepsilon T_f^3$$

当取环境温度 $T_f = 293$ K 时, 焊丝的表面散热系数 $\alpha = 82.2819$ W/(m^2·K).

2.1.2 热丝温度分布模型的验证

由热丝的温度分布解析模型, 即式(5)计算焊丝伸出长度方向上的温度分布, 与文献[6]中利用辐射测温计所测得的不同焊接电流下焊丝的温度分布进行对比, 进而验证此解析模型的准确性.

文献[6]中所选用的焊丝为 SUS3 系列的不锈钢焊丝, 直径为 1.4 mm, 送丝速度为 0.11 m/s, 焊丝伸出长度为 0.062 m. 焊接电流分别为 165, 172, 183 A 时, 由式(5)计算的结果与文献[6]中的数据进行了对比如图 2 所示.

由图 2 中的曲线可以看出来, 在电流较大时, 在近焊丝送丝位置处, 解析模型的计算结果和文献[6]中的实测结果的吻合性非常好, 焊丝上近给电点处由解析模型计算的结果和文献中实测的结果吻合性不是很好的原因在于, 此模型假设材料的物性

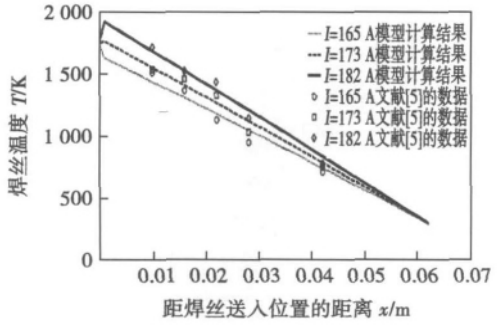

图2　解析模型计算结果与文献 [5] 测量结果对比

Fig. 2　Comparison of mathematical model with experimental data from fifth reference

参数与温度无关. 尽管在近给电点处吻合性不是很好,但计算结果与实测结果的误差在 10% 以内,满足热丝 TIG 焊热丝加热过程的分析以及焊丝温度的控制要求.

2.2　热丝温度数学模型的讨论

由式(5)可知,热丝温度分布与材料自身的热物理性能及其电性能、焊丝直径、热丝电流、送丝速度、焊丝伸出长度等因素有关. 当焊丝的材料确定之后,热丝温度分布则主要与焊丝的直径、热丝电流、送丝速度、焊丝伸出长度等因素有关. 通过以 SUS3 系列奥氏体不锈钢焊丝为例,讨论以上四个主要非物性因素对热丝温度分布的影响规律.

2.2.1　焊丝直径对焊丝温度分布的影响规律

现考虑焊丝伸出长度为 0.062 m、送丝速度为 0.05 m/s、热丝电流为 100 A 时,焊丝直径分别为 0.8,1.0,1.2,1.6,2.0,2.4 mm 的焊丝伸出部分的温度分布,如图 3 所示.

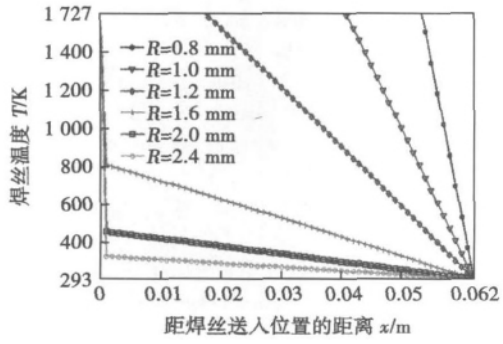

图3　不同焊丝直径下焊丝伸出部分的温度分布

Fig. 3　Temperature distribution of hot-wire extension different wire diameters

由图 3 可以看出随着焊丝直径的增大,焊丝伸出部分距给电点相同距离的温度随之降低,并且当焊丝的直径比较大时,焊丝伸出部分电阻热较小,使其对焊丝的预热作用不明显,此时熔化焊丝所需要的热量主要来自于焊接熔池和焊接电弧,这就造成了焊丝上靠近焊丝送入位置处的温度急剧升高. 当焊丝直径为 0.8,1.0,1.2 mm 时,焊丝在未到达既定的焊丝送入位置就已融化,这将导致焊丝无法正常送入熔池,最终将影响焊缝成形以及焊接质量,对于焊接生产来说,焊接工艺参数的选取应避免出现此种情况. 因此此解析模型对热丝 TIG 焊优化参数的选取具有一定的指导意义.

2.2.2　热丝电流对焊丝温度分布的影响规律

现考虑焊丝伸出长度为 0.062 m、焊丝直径为 1.2 mm、送丝速度为 0.06 m/s 时,热丝电流分别为 45,60,75,90,105,120 A 的焊丝伸出部分的温度分布如图 4 所示.

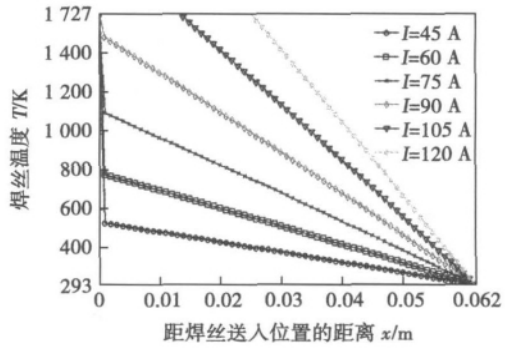

图4　不同热丝电流下焊丝伸出部分的温度分布

Fig. 4　Temperature distribution of hot-wire extension with different hot-wire current

由图 4 可以看出随着热丝电流的增大,焊丝伸出长度部分上距给电点相同距离的温度随之升高. 这是因为热丝电流越大,焊丝伸出部分产生的电阻热越多,在电阻热的预热作用下,焊丝的预热温度就越高,而此时焊接熔池以及电弧通过热传导给焊丝的热量就越少,焊丝上靠近焊丝送入位置部分的温度急剧升高的趋势变缓,但最终导致焊丝上的温度是呈逐渐升高趋势的. 并且从图 4 中可以得出,当焊丝伸出长度、焊丝直径以及送丝速度确定的时候,热丝电流有个极大值,超过此值,焊丝无法正常送入熔池.

2.2.3　送丝速度对焊丝温度分布的影响规律

现考虑焊丝伸出长度为 0.062 m、焊丝直径为 1.2 mm、热丝电流为 100 A 时,送丝速度分别为 0.05,0.06,0.07,0.08,0.09,0.1 m/s 的焊丝伸出部分的温度分布如图 5 所示.

由图 5 可以看出随着送丝速度的增大,焊丝伸

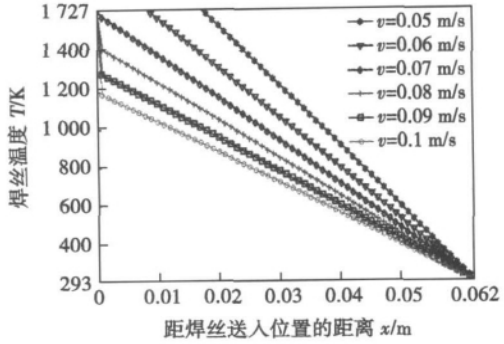

图 5 不同送丝速度下焊丝伸出部分的温度分布

Fig. 5 Temperature distribution of hot-wire extension with different wire-feeding speed

出部分上距给电点相同距离的温度随之降低. 当送丝速度较慢时，焊丝在未被送达熔池就已融化，焊丝端部会形成球状液滴，然后以类似于气体保护焊时熔滴过渡(非短路过渡)的形式滴落在工件上的非熔池区域，这将造成焊丝加热的整个回路断开，这样不仅对热丝电源会有很大的损害，而且会大大降低焊接质量. 因此送丝速度的恰当选取是获得优质焊缝的重要因素之一.

2.2.4 焊丝伸出长度对焊丝温度分布的影响规律

现考虑焊丝直径为 1.2 mm、热丝电流为 100 A、送丝速度为 0.08 m/s 时，焊丝伸出长度分别为 0.02，0.03，0.04，0.05，0.06，0.062 m 的焊丝温度伸出部分的温度分布，如图 6 所示.

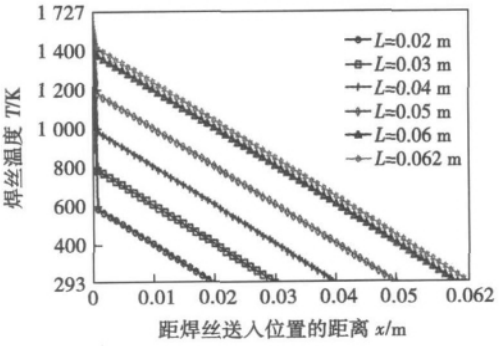

图 6 不同焊丝伸出长度下焊丝伸出部分的温度分布

Fig. 6 Temperature distribution of hot-wire extension in different length

由图 6 可以看出，随着焊丝伸出长度的增大，焊丝伸出部分距焊丝送入位置相同距离的温度随之升高. 在焊丝伸出部分的温度未发生突变之前，焊丝上的温度近似成线性关系. 在不同焊丝伸出长度下，焊丝温度的增长趋势近似相同.

3 结 论

(1) 建立了考虑热损失的电阻加热热丝 TIG 焊热丝焊丝伸出部分的准稳态温度分布数学解析模型. 通过和文献所测得的数据进行对比，文中数学模型具有一定的准确性，可用于热丝 TIG 焊热丝加热过程分析，并满足热丝 TIG 焊质量控制的要求.

(2) 分析了除焊丝材料热物性参数以外的四个主要因素，即焊丝直径、热丝电流、送丝速度以及焊丝伸出长度等对热丝温度分布的影响规律. 焊丝直径越小、热丝电流越大、送丝速度越小，焊丝伸出部分上距给电点相同距离的温度越高；焊丝伸出长度越大，焊丝伸出部分距焊丝送入位置相同距离的温度越高.

(3) 为了让焊丝顺利地被送入给定位置并保证热丝 TIG 焊的焊接效率，应保证焊丝温度分布曲线中转折点处的温度应该尽可能接近焊丝的熔点 T_m，即 $T(0.0015) \approx T_m$ 且 $T(0.0015) \leqslant T_m$.

参考文献：

[1] Shinozaki K, Yamamato M, Mitsuhata K, *et al*. Study on high-speed-welding with hot-wire TIG welding methods using pulsed current to heat filler wire(report 3) [J]. Japan Weld Society, 2007(9): 288 - 289.

[2] Shinozaki K, Yamamato M, Uchida T, *et al*. Delopment of ultra-high-speed GTA welding process using pulse-heated hot-wire [J]. Japan Weld Society, 2008(4): 228 - 229.

[3] Shinozaki K, Yamamoto M, Nagamitsu Y, *et al*. Melting phe-nome-non during ultra-high-speed GTA welding method using pulse-heated hot-wire [J]. Quartly Journal of Japan Welding Society, 2009, 27(2): 22 - 26.

[4] Mills K C, Su Y, Li Z, *et al*. Equations for the calculation of the ther-mo-physical properties of stainless steel [J]. ISIJ Internation-al, 2004, 40(10): 1661 - 1668.

[5] Shinozaki K, Yamamoto M, Mistuhata K, *et al*. Bead formation and wire temperature distribution during ultra-high-speed GTA welding method using pulse-heated hot-wire [R]. IIW Doc XII, Singapore, 2009.

[6] 武传松. 焊接热过程与熔池形态 [M]. 北京：机械工业出版社, 2007.

[7] Waszink J H, G J P M, Heuvel V D. Heat generation and heat flow in the filler metal in GMA welding [J]. Welding Journal, 1982, 61(8): 269 - 282.

[8] Nemchinsky V A. Heat transfer in an electrode during arc welding with a consumable electrode [J]. Journal of Physics. D: Applied Physics, 1998, 31: 730 - 736.

作者简介：赵福海，男，1986 年出生，硕士研究生. 主要从事高速高效焊接方法的焊接物理过程的建模与仿真模拟. 发表论文 2 篇. Email: zfhelite@126.com

通讯作者：华学明，男，副教授. Email: xmhua@sjtu.edu.cn

creases. On the basis of differences in equivalent cathode/anode drops and the welding arc characters in EN/EP polarity, the welding wire gets more energy as the EN ratio increases, so the wire melting rate is larger than DC MIG welding. At a constant wire feed speed and welding speed, the penetration depth and bead width decrease while the reinforcement becomes high as the EN ratio increases. Accordingly, AC Pulse MIG welding technology can solve the burn through problem in welding thin sheet joints and can greatly improve the gap bridging ability in lap joints. What is more, this technology can also improve the welding speed and welding bead quality for thin sheet joints.

Key words: aluminum alloy welding; AC pulse MIG welding; EN ratio; wire welding rate

Analytical model of wire temperature distribution during hot-wire TIG welding process ZHAO Fuhai[1,2], HUA Xueming[1,2], YE Xin[1,2], WU Yixiong[1,2,3] (1. Welding Engineering Institute of Material Science and Engineering Shanghai Jiaotong University, Shanghai 200240, China; 2. Shanghai Key Laboratory of Materials Laser Processing and Modification, Shanghai Jiaotong University, Shanghai 200240, China; 3. State Key Laboratory of Metal Matrix Composite, Shanghai Jiaotong University, Shanghai 200240, China). pp 97 – 100

Abstract: Based on the law of energy conservation, the mathematical model considering the effect of heat loss on the hot-wire temperature distribution was developed. The accuracy of the mathematical model was validated by comparing the calculating result with the experimental results. The effect of wire diameter, hot-wire current, wire feeding speed, and wire extension on temperature distribution of hot-wire elaborately was discussed. The results show that the mathematical model has so high accuracy that it can be used to analyze the heating process of wire and satisfies the need of controlling the welding quality. The smaller the wire diameter and wire feeding speed are, the higher the temperature of the position on the wire extension having the same distance away from the power-feeding point is. The higher hot-wire current is, the higher the temperature is. However, the larger the wire extension is, the higher the temperature of the position on the wire having the same distance away from the wire-feeding point is.

Key words: hot-wire TIG welding process; heat-loss; temperature distribution of hot-wire; mathematical analytical model

Development of flux for Sn-Zn lead-free solder HAN Ruonan[1], XUE Songbai[1], HU Yuhua[2], WANG Zongyang[1], JA Jianyi[1] (1. College of Materials Science and Technology, Nanjing University of Aeronautics and Astronautics, Nanjing 210016, China; 2. The 55th Research Institute, China Electronic Technology Group Corporation, Nanjing 210016, China). pp 101 – 104

Abstract: The speadabitity of Sn-9Zn solder on Cu substrate with four different types of flux was studied by spreading experiment method. The experimental results indicated that Sn-9Zn solder, matching the flux-A4 with stannous sulfonate (20%) as the main activator without halogen which exhibited excellent wettability. The largest spreading area was 65.7 mm^2, increased respeetively by 16.1%, 116.1%, 85.1% compared with the NH_4Cl-$ZnCl_2$, resin and water-solubility fluxes. Besides, the newly developed flux with combination of 20% stannous sulfonate and diethanolamine, succinic acid could remarkably improve the wettabiltiy of Sn-9Zn solder that the largest spreading areas were 76.5 mm^2, 72.5 mm^2 when the contents of diethanolamine, succinic acid were at 8%, 10%.

Key words: Sn-Zn; soldering flux; spreading areas

Effect of aging temperature on microstructure and properties of deposited metal for type 15-5PH precipitation hardened stainless steel QI Yanchang, ZHANG Xiaomu, PENG Yun, TIAN Zhiling (State Key Laboratory of Advanced Steel Processes and Products, Central Iron & Steel Research Institute, Beijing 100081, China). pp 105 – 108

Abstract: Aging temperature is an important aging treatment parameter of deposited metal for type 15-5PH precipitation hardened stainless steel. The welding deposited metal was conducted by gas tungsten arc welding and aging treatment was carry out at different temperature after solution treatment. After aging treatment the microstructure and properties of deposited metal were investigated. The results indicate that microstructure of deposited metal by aging treatment consists predominately of martensite, residual austenite and ε-Cu. The increasing of aging temperature results in the increasing of amount of austenite and the size of ε-Cu, the variation of ε-Cu from increasing to decreasing. The strength of deposited metal drops and toughness improves with the increasing of aging temperature due to the increasing of amount of austenite.

Key words: aging temperature; microstructure; properties; deposited metal

Structure and mechanical properties of TC4/TC17 linear friction welding joint JI Yajuan[1], LIU Yanbing[2], ZHANG Tiancang[1], ZHANG Chuanchen[1] (1. AVIC Beijing Aeronautical Manufacturing Technology Research Institute, Beijing 100024, China; 2. No. 94170 Unit of People's Liberation Army, Xi'an 710061, China). pp 109 – 112

Abstract: TC4 and TC17 titanium usually used on aero-engine blisk were studied. The microstructures were analyzed by metallograph and transmission electron microscope. The temperature during the welding process was also measured. The investigation showed that the joints included three zones, base metal (BM), thermal mechanical affected zone (TMAZ) and welding zone(W). The TMAZ microstructure was similar to base metal, alpha and beta phase were elongated along the stress direction, recrystallization occurred in the weld zone. The induced microstructures were different from the BM. The maximum temperature can reach 1 270 ℃ which exceeds the titanium beta transformation temperature. the tensile test result showed that joint tensile strength was equal to that of the TC4 at room temperature and 200 ℃, while the testing temperature is 400 ℃, the joint tensile strength can reach 95% of the TC4 base mental.

Key words: linear friction welding; titanium; microstructure; temperature